Catalysis Science & Technology

PAPER

View Article Online
View Journal | View Issue



Cite this: *Catal. Sci. Technol.*, 2014, 4, 2978

# Phosphine free SBA-15–EDTA–Pd highly active recyclable catalyst: synthesis characterization and application for Suzuki and Sonogashira reaction†

Priti Sharma and A. P. Singh*

Received 5th February 2014,
Accepted 22nd March 2014

DOI: 10.1039/c4cy00144c

www.rsc.org/catalysis

Phosphine obstructed highly efficient and reusable SBA-15–EDTA–Pd(11) has been synthesized by anchoring a Pd–EDTA complex over the surface of organo-functionalized SBA-15. The physiochemical properties of the organo-functionalized catalyst were analyzed by elemental analysis, ICP-OES, XRD, $N_2$ sorption measurement isotherms, TGA and DTA, solid state $^{13}C$, $^{29}Si$ NMR spectroscopy FT-IR, XPS DRS UV-visible, SEM and TEM. The XRD and $N_2$ sorption analyses of the synthesized catalyst confirm that the ordered mesoporous channel structure was retained even after the multistep synthetic procedures. The (100), (110) and (200) reflections in SBA-15 provide a good structural stability, an the existence of a long range order and high pore wall thickness. The TGA-DTA results reveal that the thermal stability of the synthesized catalyst SBA-15–EDTA–Pd(11) was maintained at higher temperature. The organic moieties anchored over the surface of the SBA-15 and inside the pore wall were demonstrated by solid state $^{13}C$ NMR and FT-IR spectroscopy. Further, solid state $^{29}Si$ NMR spectroscopy provides information about the degree of functionalization of the surface silanol groups, of the SBA-15 with organic moieties. The electronic environment and oxidation state of the Pd metal in the SBA-15–EDTA–Pd(11) were monitored by XPS, and DRS UV-visible techniques. Moreover, the morphologies and topographic information of the synthesized catalyst were confirmed by SEM and TEM spectroscopy. The synthesized catalyst SBA-15–EDTA–Pd(11) was screened for the Suzuki and Sonogashira coupling reactions and shows a higher catalytic activity with higher TON (turn over number). The anchored solid catalyst can be recycled efficiently and reused five times, without a major loss in the reactivity.

## Introduction

Various homogenous complexes are widely used for organic transformations; however, the separation and recycling of the rather expensive catalysts imparts difficulties. The heterogenization of such homogenous catalysts on solid supports can mitigate these problems. Furthermore, heterogeneous catalysts have clear advantages over their homogeneous counterparts; they can be easily separated from the reaction medium. "Heterogeneous catalytic system includes polymer/dendrimer supported palladium catalysts palladium on carbon palladium supported metal oxides clays and molecular sieves".[1] Since the synthesis of ordered mesoporous materials in 1992 sparked worldwide interest in the field of heterogeneous catalysis and separation science; SBA-15 has become the most popular member of the group, possessing extremely high surface areas, ease of accessibility, uniform pore sizes and stability.[2]

To extend the applicability of SBA-15 materials, it is necessary to modify the surface by organic functional groups, to anchor metals and metal complexes. The grafting of functional organosilanes by using the surface hydroxyl groups as the anchor points has been widely used. Furthermore, the leaching of the active site can also be avoided as the organic moieties are covalently attached to the inorganic support.

Palladium complexes, with or without phosphine ligands, can catalyze C–C coupling reactions. The phosphine-assisted approach is the classical and well-established method,[3] which gives excellent results in the majority of cases; whereas phosphine ligands are expensive, toxic, and unrecoverable. Additionally, a major drawback of phosphine ligands in a catalytic reaction is the oxidation of phosphine to a phosphine oxide, as well as cleavage of the P–C bond, causing degradation of the catalytic cycle. In large-scale industrial applications, phosphines might be a more serious economical burden than even palladium itself, which can be recovered at any stage of the production, or from the waste. Therefore, the

*Catalysis Division, CSIR-National Chemical Laboratory, Pune 411008, India. E-mail: ap.singh@ncl.res.in; Fax: (+)91 20 2590 2633; Tel: (+)91 20 2590 2497*

† Electronic supplementary information (ESI) available: Suzuki, Sonogashira product $^1H$, $^{13}C$ NMR, details of experimental section, pore size distribution plot, TGA, DTA plot, X-ray photoelectron spectroscopy (XPS), solvent, temperature and base optimization for the Suzuki and Sonogashira coupling reaction. See DOI: 10.1039/c4cy00144c

development of phosphine-free catalysts for C–C bond-forming reactions would be an important topic, of interest to current industrial research.[4]

The accurate selection of the ligands is the key factor for the synthesis of the complex. Recently, a number of nitrogen based compounds in phosphine free conditions have commonly been used as the ligand, such as C based heterocyclic carbenes, C–N based 2-aryl-2-oxazolines, aryl (heteroaryl) oximes, arylimines, *N*,*N*-based diazobutadienes, DMG and salen complexes.[5] However, these ligands are not easily available and contain tedious and expensive synthesis processes and are hardly stable in the catalytic systems. Therefore, a simple, easily accessible, stable catalyst is desired for these high temperature reactions.

Cross coupling reactions are one of the broadest areas for the synthesis of symmetrical and unsymmetrical binary compounds, which are the key components of the several natural products, as well as in the field of engineering materials, such as conducting polymers, molecular wires and liquid crystals.[6] Among the basic types of palladium catalyzed transformations, the Suzuki and Sonogashira reactions related chemistry occupy a special place.[7] The Suzuki cross-coupling reaction of organoboron reagents with organic halides represents one of the most versatile and straightforward methods for carbon–carbon bond formation. The reaction is largely unaffected by water, tolerating a large range of functionality and yielding non-toxic byproducts. Furthermore, the Sonogashira coupling of phenyl acetylenes and aryl halides is one example of a palladium catalyzed reaction that allows the connection of a C≡C triple bond substituent to an aromatic ring.

In 2005, Korolev *et al.* described the synthesis of a $PdCl_2$–EDTA complex as a homogeneous catalyst for the Suzuki–Miyaura reaction in water.[8] However, this catalytic system was not stable enough to store for a long time period and unfortunately, no catalyst recovery was possible. In this context, we decided to immobilize the Pd-complex on the surface of an organo-functionalized SBA-15, in order to recycle the catalyst. Herein, we report grafting of Pd–EDTA complex, and its derivatives into SBA-15 phases and their catalytic properties in the Suzuki and Sonogashira coupling reactions, as a heterogeneous catalyst. The immediate goals of our study were (i) to evaluate the heterogenization method of the Pd–ethylenediaminetetraacetic acid complex over an organo-modified mesoporous SBA-15 support, (ii) to measure the catalytic properties in the Suzuki and Sonogashaira C–C coupling reactions (iii) to optimize the reaction parameters, such as the temperature, solvent and base in the both coupling reactions, (iv) to determine the extent of the stability of the catalysts, as well as their recycling properties.

## Results and discussion

The heterogenized palladium catalyst, SBA-15–EDTA–Pd, was obtained by the procedure outlined in Scheme 1. Starting from the synthesis of SBA-15 and surface modification was achieved by a post synthesis grafting method (Scheme 1A) furthermore, free –OH groups present in $NH_2$–SBA-15 were protected (Scheme 1B) by published procedure.[21] Finally Pd–EDTA complex was covalently grafted over the organo-modified surface of the SBA-15.[8] The products were dried and characterized systematically by nitrogen sorption isotherms; cross polarization magic angle spinning (CPMAS) NMR and infrared spectroscopies; elemental analysis; and thermogravimetric and differential thermogravimetric (TGA-DTA) analysis to gain complete structural and compositional information.

The XRD patterns of (a) calcined SBA-15, (b) –OH protected $NH_2$–SBA-15 and (c) Pd–EDTA–SBA-15(11) complexes are visualized in Fig. 1 and (a) SBA-15–EDTA–Pd(7), (b) SBA-15–EDTA–Pd(11), (c) SBA-15–EDTA–Pd(15) in Fig. S1 (ESI†). The typical hexagonal phase of the SBA-15 [main (100), (200), and (210)] reflections are clearly visible in the calcined SBA-15. In all the samples, the (110) reflection is more intense than the (200) reflection. It favors a more complete condensation of the wall structure, due to the higher temperature preferred in the hydrothermal synthesis and further calcinations. As evident from Fig. 1 the XRD patterns of the samples synthesized after treatment with 3-APTMS and $[(MeO)_2SiMe_2]$ are almost similar to the parent SBA-15 sample, with a small decrease in the overall intensity to the (100), (110) and (200) reflections. From the XRD pattern, it is clear that after the anchoring of the Pd–EDTA complexes with different weight% ratios (7%, 11%, 15%) an inconsequential decrease in the peak intensities to the (100), (110) and (200) reflections was observed without changing the peak positions (Fig. S1†). This perseverance of the peak positions indicates that even the presence of a large amount of Pd–EDTA complex moieties, by the partial filling inside the mesopores, is less detrimental to the quality of the SBA-15 material.[9] The persistence of the (100), (110) and (200) reflections (Fig. 1) not only proved the structural stability and existence of a long range ordering to the mesophase, but also the survival of the undisturbed pore wall thickness, even after a number of treatments with organic molecules in solvents.

The nitrogen adsorption–desorption results of the calcined SBA-15 and SBA-15–EDTA–Pd(7), SBA-15–EDTA–Pd(11), SBA-15–EDTA–Pd(15) samples and their corresponding pore size distribution curves are plotted in Fig. 2 and S2,† respectively. The $N_2$ adsorption–desorption isotherms of all the samples show a type IV isotherm. The surface area, average pore diameter, pore volume and wall thickness were observed for the calcined SBA-15 and SBA-15–EDTA–Pd(7), −11 and −15 derivatives samples and are summarized in Table 1. All the samples show type IV adsorption isotherms, according to the IUPAC classification, indicating the uniformity of the mesopores due to capillary condensation of $N_2$ within the mesopores with a completely reversible nature, uniformly sized mesopores, with a capillary condensation step at $P/P_o$ = 0.3–0.4.

The total surface area, average pore diameter and pore volume observed for the calcined SBA-15, SBA-15–EDTA–Pd(7), SBA-15–EDTA–Pd(11) and SBA-15–EDTA–Pd(15) were found

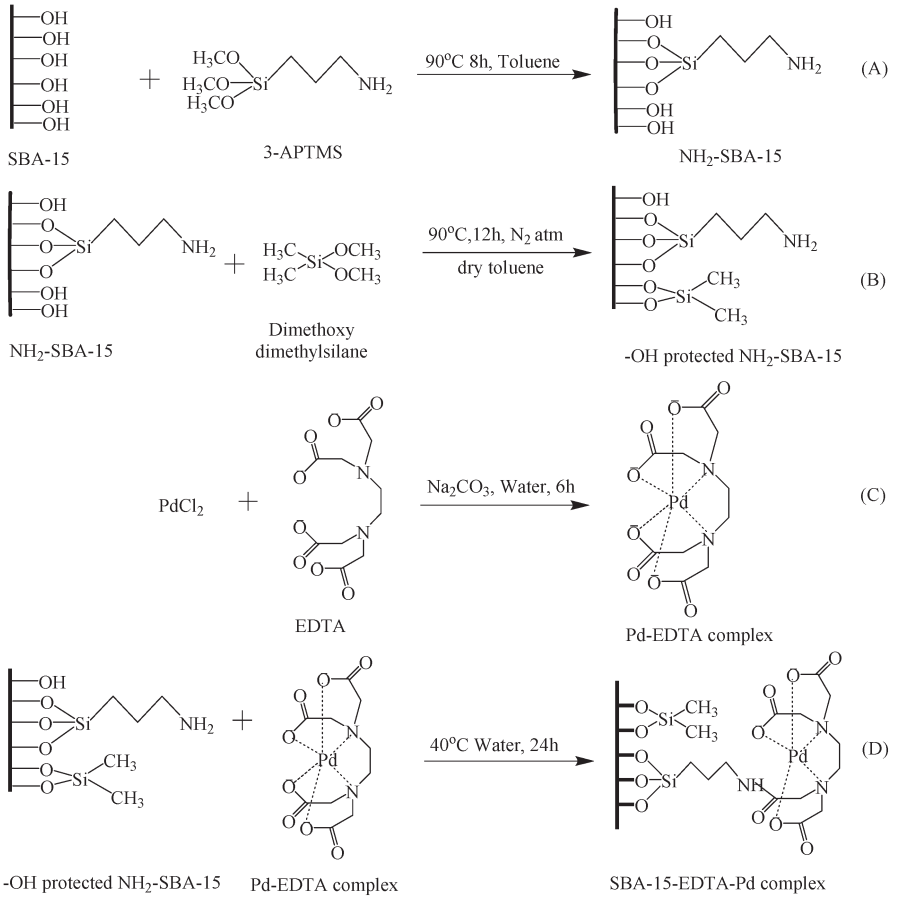


**Scheme 1** Schematic diagram of SBA-15 functionalization and heterogenization of Pd–EDTA–SBA-15. 1(A) Amino ($-NH_2$) functionization, 1(B) capping of SBA-15, 1(C) Pd–EDTA complex formation, 1(D) anchoring of Pd–EDTA complex over modified surface of SBA-15.

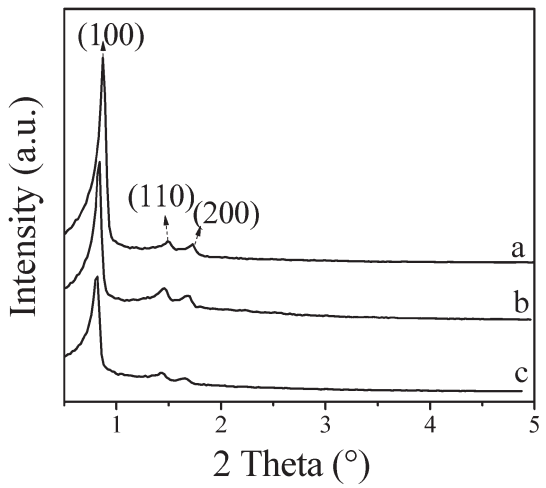


**Fig. 1** XRD pattern of (a) calcined SBA-15 (b) –OH protected $-NH_2$–SBA-15 (c) SBA-15–EDTA–Pd(11).

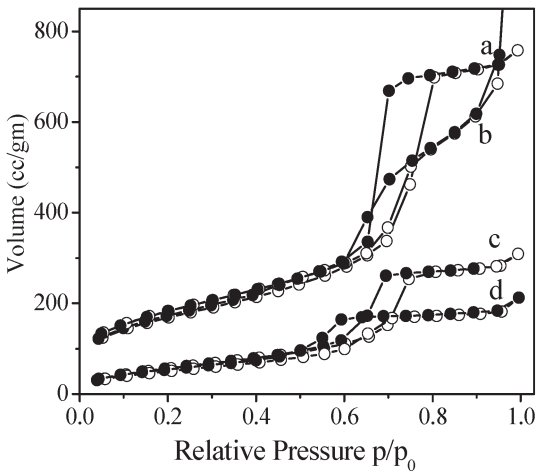


**Fig. 2** Nitrogen adsorption–desorption isotherm of (a) calcined SBA-15, (b) SBA-15–EDTA–Pd (7), (c) SBA-15–EDTA–Pd(11), (d) SBA-15–EDTA–Pd(15).

to be 739 $m^2\ g^{-1}$, 65 Å, 1.173 $cm^3\ g^{-1}$, 665 $cm^3\ g^{-1}$, 64.3 Å, 0.439 $cm^3\ g^{-1}$, 363 $m^2\ g^{-1}$, 56 Å, 0.478 $cm^3\ g^{-1}$ and 187 $m^2\ g^{-1}$, 48.5 Å, 0.36 $cm^3\ g^{-1}$, respectively. The decrease in the total mesoporous surface area (10%, 50%, 74%), pore diameter (2%, 13%, 26%) and pore volume (62%, 59%, 69%) after metal Pd–EDTA complex immobilization over organo-modified SBA-15 is indicative of the grafting of the complex Pd–EDTA inside the channels of the mesoporous SBA-15. It is clear from Table 1 that even though silylation procedures changed the textural properties of the mesoporous material,

 

**Table 1** Textural properties of mesoporous calcined SBA-15 & SBA-15–EDTA–Pd

| Sample | N[a] (wt.%) | Loading of Pd[b] (wt.%) | | BET surface area ($m^2\ g^{-1}$) | Average pore diameter ($D_P$) (Å) | Pore volume ($V_p$, $cm^3\ g^{-1}$) |
|---|---|---|---|---|---|---|
| | | Input | Output | | | |
| Calcined SBA-15 | | | | 739 | 65 | 1.17 |
| SBA-15–EDTA–Pd(7) | 2.2 | 7 | 5.7 | 665 | 64 | 0.43 |
| SBA-15–EDTA–Pd(11) | 2.5 | 11 | 6.2 | 363 | 56 | 0.47 |
| SBA-15–EDTA–Pd(15) | 4.3 | 15 | 10.8 | 187 | 48 | 0.36 |

[a] Calculated based on elemental (nitrogen) analysis value. [b] Input is based on the amount of Pd during synthesis reaction; output is based on the ICP-OES analysis.

the decrease is more prominent after Pd–EDTA complex immobilization, since the bulkier organic moieties inside the pore channels occupy a large area of the void space. The capillary condensation steps of SBA-15–EDTA–Pd(7), SBA-15–EDTA–Pd(11), and SBA-15–EDTA–Pd(15) due to anchoring of Pd–EDTA complexes are reduced to lower $P/P_o$ values. The shift to a slightly lower partial pressure shows a possible reduction in the pore size and a partial distortion in the pore arrangement, consistent with the XRD results. It is known that the inflection position in the $N_2$ sorption isotherm depends on the diameter of the mesopores and the sharpness usually indicates the uniformity of the mesopores, due to capillary condensation of $N_2$ within the mesopores.

The presence of isolated surface silanols, hydrogen bonded hydroxyl groups, anchored on the complex Pd–EDTA are evidenced from the IR spectrum of the calcined SBA-15 and its modified samples. Fig. 3 shows the FT-IR spectra of (a) EDTA, (b) calcined SBA-15, (c) –OH protected $NH_2$–SBA-15, (d) SBA-15–EDTA–Pd(7), (e) SBA-15–EDTA–Pd(11), (f) SBA-15–EDTA–Pd(15). In the visualized IR spectrum of calcined SBA-15 and –OH protected $NH_2$–SBA-15 the *v*–OH stretching vibrations observed in the range 3600–3400 $cm^{-1}$ region are attributed to the hydrogen-bonded silanol groups and the sharp band at 3757 $cm^{-1}$ corresponds to the isolated surface silanol

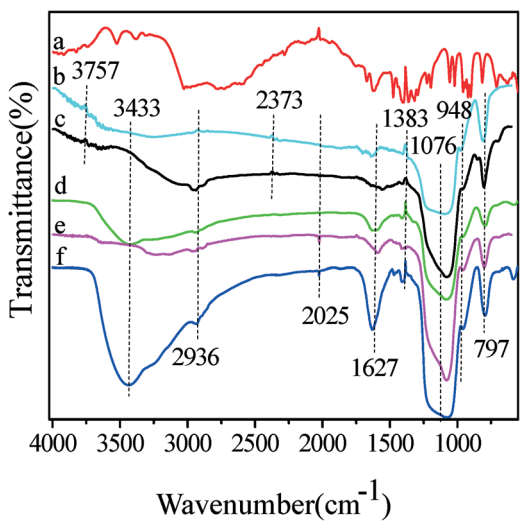


**Fig. 3** FT-IR spectrum of (a) EDTA, (b) calcined SBA-15, (c) –OH protected $NH_2$–SBA-15, (d) SBA-15–EDTA–Pd(7), (e) SBA-15–EDTA–Pd(11), (f) SBA-15–EDTA–Pd(15).

groups (Fig. 3b) In the present analysis, after 3-APTMS functionalization, a sharp decrease in the intensity of peak at 3757 $cm^{-1}$ with a peak shift to a lower value is seen, demonstrating the role of the surface silanols in modifications (Fig. 3c). In Fig. 3 the bands observed near 797 $cm^{-1}$ and 1076 $cm^{-1}$ are due to the symmetric and asymmetric vibrations of the Si–O–Si group, respectively.[10] Two strong bands were observed in the case of SBA-15–EDTA–Pd(11) complexes at 1620 and 1587 $cm^{-1}$; these correspond to the C–O stretching vibrations and N–H bending vibrations, respectively.[11] Further, the intensity of the C–O stretching vibrations and N–H bending vibrations increases as the loading of Pd–EDTA complex increases. Since the Pd–EDTA was anchored over the modified surface of the SBA-15, the band at 3294 $cm^{-1}$ ascribed to the $NH_2$ stretching vibrations disappeared, while a broad weak band at 3257 $cm^{-1}$ was observed, which is attributed to the stretching vibration of $-[NH_3]^+$ resulting from the EDTA modification.[12] This broad band is much broader in the case of the SBA-15–EDTA–Pd(15) catalyst, which might be due to the higher loading of the Pd–EDTA complex. Further, new bands at 1383 and 1627 $cm^{-1}$ were also observed for the Pd–EDTA modified SBA-15, which are attributed to the –COO– group symmetrical and asymmetrical stretching vibrations, respectively. These observed results indicate that all the SBA-15–EDTA–Pd complexes, along with different loading, are systematically synthesized.

Fig. 4 show the solid state $^{13}C$ CP/MAS NMR spectra of (a) $NH_2$–SBA-15, (b) –OH protected – $NH_2$–SBA-15, (c) SBA-15–EDTA–Pd(11). In the solid state $^{13}C$ CP/MAS NMR spectra of $NH_2$–SBA-15, –OH protected $NH_2$–SBA-15 and SBA-15–EDTA–Pd(11), the peak observed at 9.3 ppm can be accounted for by the carbon (C1) atom bonded to the silicon. The signal at 21.3 ppm corresponding to a methylene carbon (C2) and the signal at 42.5 ppm can be attributed to the carbon atom attached to the $NH_2$ group (Fig. 4a). After the –OH group protection of $NH_2$–SBA-15 by dimethoxydimethylsilane, along with all three peaks of $NH_2$–SBA-15, one extra peak is clearly visible at −2.2 ppm, which corresponds to the methyl group attached the to capping agent dimethoxydimethylsilane (Fig. 4b). Additionally, no peak was observed for the methoxy group, which confirms the successful grafting of the 3-APTMS over the support (SBA-15). Two consecutive peaks, observed at 171 ppm and 180.6 ppm, correspond to the carbon atoms of the amide group formed due to the carboxylic group being anchored to the linker 3-APTMS of the SBA-15.

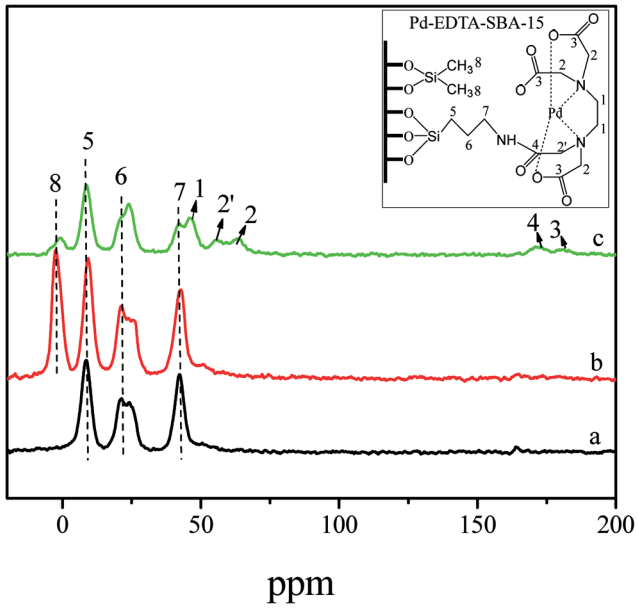


Fig. 4 Solid state $^{13}C$ CP/MAS NMR spectrum of (a) $NH_2$–SBA-15, (b) –OH protected –$NH_2$–SBA-15 (c) SBA-15–EDTA–Pd(11).

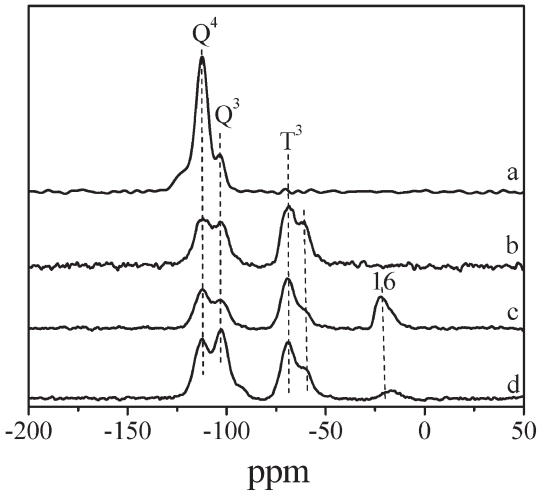


Fig. 5 Solid state $^{29}Si$ CP/MAS NMR spectrum of (a) calcined SBA-15, (b) $NH_2$–SBA-15, (c) –OH protected –$NH_2$–SBA-15 (d) SBA-15–EDTA–Pd(11).

Furthermore, another peak observed in the case of SBA-15–EDTA–Pd(11), at 63.85 ppm, corresponds to the carbon of the ethylene group in EDTA, which is directly attached to the amide group and the peak at 55.4 ppm is due to the ethylene group, which is directly attached to the carboxylic acid group (Fig. 4c). The reason for the appearance of two types of peak for the carboxylic acid might be that all the carboxylic groups did not get anchored over the 3-APTMS modified surface of the SBA-15.

The $^{29}Si$ MAS NMR spectra of (a) calcined SBA-15, (b) $NH_2$–SBA-15, (c) –OH protected –$NH_2$–SBA-15, (d) SBA-15–EDTA–Pd(11) are exhibited in Fig. 5. The peaks seen in the spectra, at −112, −102, −68 and −61 ppm, are usually assigned to the $Q^4$ [$Si(OSi)_4$, siloxane], $Q^3$ [$Si(OH)(OSi)_3$, single silanol] and $T^3$ [$SiR(OSi)_3$] sites, respectively (Fig. 5a–d). The calcined SBA-15 sample shows the presence of broad resonance peaks from −126 to −98 ppm, indicative of a range of Si–O–Si bond angles, and it is noteworthy that the sample contains large amounts of $Q^4$ sites, showing a high framework cross-linking.[13] The low intensity in the $Q^3$ value shows that these silanol groups are highly accessible to the silylating agents (Fig. 5a). In the –OH protected-$NH_2$–SBA-15, the Si spectrum shows one extra peak at −68.48 ppm, due to the capping agent dimethoxydimethylsilane, which is assigned to a mixture of $T^3$ [$SiR(OSi)_3$] and $T^2$ [$Si(OH)R(OSi)_2$] organosilicon, respectively. The peak at −16.87 ppm corresponds to the Si of the (dimethoxydimethylsilane) capping agent (Fig. 5c). After protection of the –OH group in $NH_2$–SBA-15 by dimethoxydimethylsilane, it is clearly visible that the $T^2$ site [$Si(OH)R(OSi)_2$] disappeared, along with the appearance of a new peak at 16 ppm. These two significant changes evidently proved the free silanol group of $NH_2$–SBA-15 the $T^2$ site [$Si(OH)R(OSi)_2$] becomes blocked by a condensation with the methoxy group of the dimethoxydimethylsilane (Fig. 5c). The absence of the $T^0(SiC(OH)_3$ sites confirms that the EDTA–Pd complex is covalently anchored to the modified surface of the SBA-15 (Fig. 5d).

The thermal stability of all the synthesized materials was studied by thermogravimetric analysis (TGA), under an air atmosphere, from ambient temperature to 1000 °C with a temperature increment of 10 °C $min^{-1}$. The TGA plots of all the synthesized and modified SBA-15 samples show an approximately 5% weight loss below 120 °C, caused by the desorption of physisorbed water molecules (Fig. S3†). In the TGA plot, a loss of ~42 weight% from the as-synthesized SBA-15 was observed between 132 °C and 195 °C, which corresponds to the removal of the trapped surfactant within the closed pores (Fig. S3,† A, B, a). In comparison, nearly no weight loss in the TGA and DTA was observed in the calcined SBA-15 between 132 °C and 195 °C, which indicates the complete removal of surfactant from SBA-15 (ref. 14) (Fig. S3,† A, B, b). These data evidently support the complete removal of the organic surfactant from the calcined SBA-15. The TGA results of the –OH protected $NH_2$–SBA-15 sample shows a weight loss in three steps. In the first step, a weight loss between 70 °C and 150 °C corresponds to the loss of loosely bounded water, adsorbed moisture, which is clearly evidenced by the small exothermic peak of the DTA. In the second step, a weight loss was observed in the region of 245–385 °C. The TGA analysis and a sharp visible exothermic peak in the DTA analysis in the same temperature region (245–385 °C) are attributed to 3-APTMS. The TGA plot of –OH protected $NH_2$–SBA-15 quantitatively shows an ~21.27% weight loss, which is greater than the calcined SBA-15; this strongly supports the successful anchoring of the 3-APTMS over SBA-15. The third weight loss visible in the TGA analysis in the 380–480 °C range corresponds to the removal of dimethoxydimethylsilane [$(MeO)_2SiMe_2$], which is evidently supported by the DTA analysis showing one strong exothermic peak in the same temperature range (Fig. S3,† B, c). In

 

the case of the heterogenized metal complex SBA-15–EDTA–Pd(11) one extra peak was observed along with two peaks shown in the –OH protected $NH_2$–SBA-15, in the region of 437–556 °C assigned to the Pd–EDTA complex. Note that decomposition of the Pd–EDTA complex occurred at an elevated temperature revealing the high thermal stability of the complex. A direct comparison of the weight loss in the case of heterogenized SBA-15–EDTA–Pd(11), and in the capped amino functionalized SBA-15 shows an ~7 weight% loading of the complex material (Fig. S3,† A, B, d).

A TEM image of the calcined SBA-15 and SBA-15–EDTA–Pd(11) provide structural evidence that the material is organized into ordered arrays of two-dimensional hexagonal mesopores (Fig. 6). A significant difference in the TEM patterns was not observed between the two Fig. 6A, B. However, after the anchoring of the EDTA–Pd complex inside the mesoporous channels of SBA-15 the image show distinct, deep contrasting *meso* parallel channels, with respect to the light shaded surface. This might be interpreted as being due to the presence of the EDTA–Pd complex inside the SBA-15, but not on the surface. If the EDTA–Pd complex was anchored on the surface of the functionalized SBA-15, then the high-contrast dark *meso* parallel channels would have appeared along the boundary of the visualized SBA-15 and not inside the porous body, as observed previously by Shephard *et al.*[15] Thus, the immobilization of the Pd-complex inside the pore-channels, by anchoring to the interior walls of these porous channels may be supported by the TEM analysis.

The morphologies of the calcined SBA-15 and SBA-15–EDTA–Pd(11) are shown in Fig. 7A, B, respectively. The calcined SBA-15 shows uniform arrays of mesochannels and clearly, a molecular-scale periodicity in the SEM images. Further, the SBA-15–EDTA–Pd(11) is demonstrated to be a molecular-based material; the large molecular system becomes denser in comparison to the calcined SBA-15 after the Pd–EDTA complex is anchored over the mesoporous surface.

X-ray photoelectron spectroscopy (XPS) is a powerful tool to investigate the electronic properties of the species formed on the surface, such as the electronic environment, *e.g.* oxidation state and or multiplicity influences in the binding energy of the core electron of the metal. The synthesized material SBA-15–EDTA–Pd(11) was characterized by X-ray photoelectron spectroscopy (XPS) to ascertain the oxidation state of the Pd species. In Fig. S4 (ESI†) the Pd binding energy of the SBA-15–EDTA–Pd(11) exhibits two strong peaks, centered at 336.7 eV and 341.5 eV, respectively, which are assigned to the Pd $3d_{5/2}$ and Pd $3d_{3/2}$ signal, respectively. The observed peaks correspond to the $Pd^{2+}$ oxidation state in the synthesized SBA-15–EDTA–Pd(11). According to the literature, the pure $PdCl_2$ metal salt binding energy for the Pd $3d_{3/2}$ and Pd $3d_{5/2}$ orbitals appear at 342.8 and 337.6 eV, respectively.[16] In comparison to the literature values, the synthesized SBA-15–EDTA–Pd(11) shows a shift in binding energy of Pd towards a lower value *viz.* 341.5 Pd $3d_{3/2}$ and 336.7 eV Pd $3d_{5/2}$, respectively.[17] The shift in the binding energy towards lower values indicates that the Pd state in SBA-15–EDTA–Pd is a more electron rich state than the $PdCl_2$. The reason for this might be the possibility of an electron donation from the EDTA to the palladium and it suggests a strong interaction between the Pd metal species and the EDTA ligand was present in the SBA-15–EDTA–Pd catalyst. These results are in agreement with the UV-vis observations.

Diffuse reflectance UV-vis measurement is a useful technique to obtain information about the oxidation state of an incorporated metal species. The UV-vis spectra of (a) calcined SBA-15, (b) SBA-15–EDTA–Pd(7), (c) SBA-15–EDTA–Pd(11), (d) SBA-15–EDTA–Pd(15) are shown in Fig. 8. Calcined SBA-15 shows the characteristic absorption at 254 nm, which corresponds to the siliceous material (Fig. 8a). The diffuse

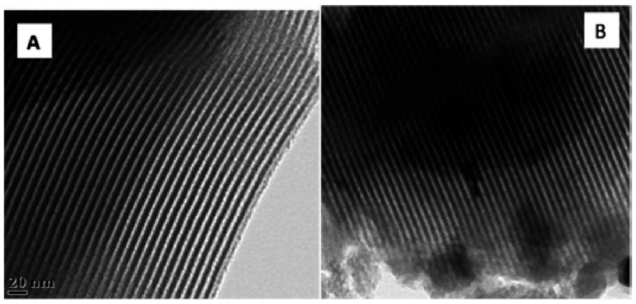


Fig. 6 TEM images of calcined (A) SBA-15 and (B) SBA-15–EDTA–Pd(11).

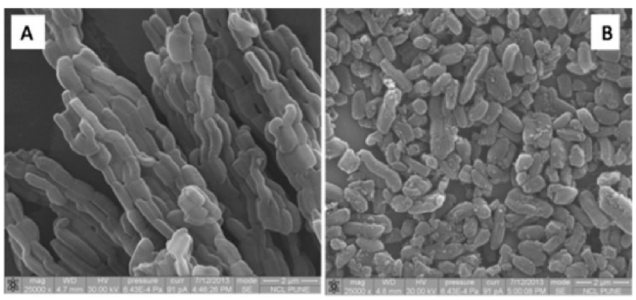


Fig. 7 SEM images of calcined (A) SBA-15 and (B) SBA-15–EDTA–Pd(11).

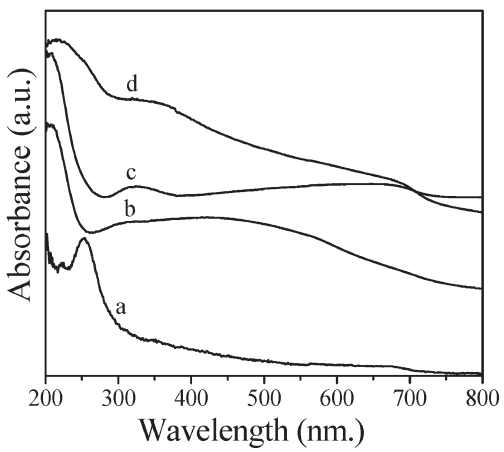


Fig. 8 UV absorbance spectra of (a) calcined SBA-15, (b) SBA-15–EDTA–Pd(7), (c) SBA-15–EDTA–Pd(11), (d) SBA-15–EDTA–Pd(15).

reflectance spectra (200–800 nm) of the SBA-15–EDTA–Pd (Pd–EDTA loading 7, 11, 15%) catalysts display nearly identical features in the absorption bands in the UV region in the range 205–680 nm, with reference to a $BaSO_4$ standard. The UV visible spectra of the SBA-15–EDTA–Pd (Fig. 8a–c) shows characteristics bands at 205–290 nm and 325–362 nm and a broad peak at 682 nm. The weak bands in the 205–290 nm region are assigned to the weak p–p* transitions (Fig. 8b–d). The bands in the 325–362 nm region are assigned to the d–d transition of the metal;[18] this strongly supports the Pd(II) oxidation state. Another band appears at 682 nm, which might be due to an n–p* transition after incorporation of the Pd–EDTA over the modified surface of the SBA-15.

### Suzuki coupling

The catalysts SBA-15–EDTA–Pd with different wt.% loadings of Pd–EDTA (7%, 11%, 15%) were screened in the Suzuki coupling reaction using the following reaction conditions: arylboronic acid (1.5 mmol), aryl halide (1 mmol), potassium carbonate (3 mmol), DMF (3.5 ml), SBA-15–EDTA–Pd (15 mg) at 120 °C. The conversion of iodobenzene and TON with respect to Pd loading were found to be 70%, 99%, 99% and 100, 130.2 and 74.2, respectively. The reaction proceeds at the active Pd metal centre. Further, the TON increases from SBA-15–EDTA–Pd(7) to SBA-15–EDTA–Pd(11) and thereafter decreases.

The heterogeneous Suzuki cross-coupling of a boronic acid with an aryl iodide may proceed through a catalytic cycle, analogous to that proposed for homogeneous palladium catalysts.[19] In the first step of the reaction insight, an oxidative addition of the aryl halide ArX (**2**) to the SBA-15–EDTA–Pd(11) (**1**) complex provides an SBA-15 bound aryl palladium(II) complex (**3**). The leaving anion adds to the metal center, to give the intermediate (**3**). The displacement of a halide ion (X) from SBA-15-L-(Ar–Pd–X) (**3**), to give the more reactive organopalladium alkoxide SBA-15-L-(Ar–Pd–$CO_3K^+$) or organopalladium hydroxide (R–Pd–OH), depends on the base used. Further, in the second step of the reaction mechanism, transmetalation between the SBA-15-L-(Ar–Pd–$CO_3K^+$) aryl palladium(II) complex (**6**) and the boronic acid (**7**) provides the SBA-15-L-($Ar^1$–Pd–Ar) reaction intermediate (**10**), with the subsequent removal of the byproduct $B(OH)_2(CO_3^-K^+)_2$ (**9**). In the last step of the reaction mechanism, the reductive elimination of biphenyl $Ar^1$–Ar (**11**) from the unsymmetrical intermediate (**10**) regenerates the SBA-15-L-Pd (**1**) complex.

Since the mechanism of the Suzuki coupling reaction is a multistep procedure, a small variation in the physical and reaction parameters can change the product yield and rate of the reaction drastically. Hence, the influences of the solvent, reaction temperature and various bases were evaluated on the product yield using SBA-15–EDTA–Pd(11) as the catalyst with iodobenzene and boronic acid.

In order to probe the role of the solvents in the Suzuki coupling reaction, a series of solvents, such as DMSO, DMF, HMPA, THF, 1,4-dioxane, and toluene were used, in the presence of the base potassium carbonate ($K_2CO_3$) at 120 °C, in a model reaction of the Suzuki coupling between iodobenzene and boronic acid. Among all the used solvents, DMF, DMSO and NMP were able to give a significant yield (85–100%) in a 5 h reaction time period (Fig. S5†). However, the non-polar or less polar solvents such as THF and toluene progress with a strong rationale for the intermediate stabilization *via* the coordinating ability and the polarity. From the obtained results of the solvent optimization for the conversion of iodobenzene, the reactivity order emerged as follows: DMF (100%) > DMSO (89%) > NMP (83%) > THF (39%) > toluene (17%) > 1,4-dioxane (15%) > xylene (10%), respectively (Fig. S5†). In addition, the conversion of iodobenzene was also carried out using SBA-15–EDTA–Pd(11) in the presence of water as the solvent under similar reaction conditions. The yield of the biphenyl was found to be 33 wt.% in a 12 h reaction time. Since after the oxidative addition of the aryl halide, charge separation would take place at the Pd metal centre to a much greater extent. To stabilize the generated high charge during the oxidative step at the Pd centre more coordination is required which is possible from the high polar solvents. The Suzuki coupling reaction of iodobenzene (1 mmol) and a boronic acid (1.5 mmol) in the presence of $K_2CO_3$ using the solvent DMF (3.5 ml) over the SBA-15–EDTA–Pd(11) (15 mg) catalyst was examined to see the influence of the temperature in the range 60 °C to 120 °C on the product yield (Fig. S6†). A lower temperature does not favour the formation of the product (biphenyl); however the yield of the biphenyl increased sharply with an increase in the reaction temperature and reached the value of 99% in 6 h at 120 °C. Generally, the coupling reaction was favoured at high temperature, since a high activation energy is required to dissociate the aryl halide bond at the oxidative addition step. It is noteworthy to mention here that no biphenyl product was obtained below 55 °C. Hence, the optimum reaction temperature with respect to conversion towards the biphenyl product, under present reaction conditions, was found to be 120 °C (Fig. S6†).

Various bases such as NaOH, $NaHCO_3$, $K_2CO_3$ and $NEt_3$ were screened for the reaction. Among all the used bases, organic bases like triethylamine ($NEt_3$) were found to be unreactive in comparison to the inorganic bases. The order of reactivity of the iodobenzene in the presence of various bases could be arranged in the decreasing order as: $K_2CO_3$ (100) > NaOH (60) > $NaHCO_3$ (45) ≫ $NEt_3$ (32). It is clear that the reactivity of $K_2CO_3$ was found to be quite high among the used inorganic bases (Fig. S7†). Potassium carbonate was able to give a 95% yield of the coupled product (biphenyl) in 5 h at 120 °C. The Suzuki coupling reaction is known to be affected by salt particles, yet their mode of action has not been completely clarified. According to one hypothesis,[20] in the reaction, the anions at the surface of the solid salt particles act as electron donors for the Pd metal centre, which increase the electron density of the Pd metal centre. This effect could promote the oxidative step, to form the intermediate Ar–Pd–X (**3**). Therefore, the reaction is

 

accelerated because this is the rate determining step. In other words, the electron-donation effect could enhance the activity of the catalyst with an increase in the electron density of the Pd.

The characteristics of the organoboron reagent (*i.e.*, high selectivity in cross-coupling reactions, stability, non-toxic nature, and tolerance towards functional groups) often give the Suzuki coupling a practical advantage over other cross-coupling processes. After optimizing the reaction parameters of the Suzuki coupling reaction between iodobenzene and phenyl boronic acid, several substituted and non-substituted aryl halides were employed in the reaction and the results are summarized in Table 2. The desired corresponding products were obtained in good yields, with high TONs. As shown in Table 2, the Suzuki coupling reaction of phenyl boronic acid with a variety of aryl halided proceeds smoothly under mild reaction conditions, giving the corresponding coupled products in high yields (75%–99%) (Table 2, entries 1–10).

Monosubstituted aryl halides, such as chlorobenzene, bromobenzene and iodobenzene with phenylboronic acid gave 71%, 83%, 98% yields of the biphenyl and the corresponding TON were found to be 81.2, 94.9 and 128.9, respectively (Table 2, entries 1, 2, 3). In the step of the oxidative addition of the catalytic cycle of the halogenated (X = Cl, Br, I) substrates, coupling reactions involving these substrates typically decrease in the order R–Cl > R–Br > R–I. This can be explained in terms of the R–X bond dissociation enthalpies (BDE). For example, the X–Ph BDE ranges from X = Cl 95.5 ± 1.5 kcal $mol^{-1}$; X = Br 80.4 ± 1.5 kcal $mol^{-1}$ to X = I 65.0 ± 1 kcal $mol^{-1}$. It is evident from Table 2 that the reactivity of the aryl chloride and bromides with phenyl boronic acid were found to be lower than aryl iodides and require comparatively longer reaction times for the completion of the reaction.

Furthermore, electron rich and electron poor aryl halides react smoothly with phenylboronic acid in similar reaction conditions. Electron poor aryl halides like 4-chloronitrobenzene, 4-bromonitrobenzene and 4-iodonitrobenzene with phenyl boronic acid gave coupled product (4-nitro biphenyl) in 98%, 99%, 95% with TON 128.9, 130.2, 125, respectively (Table 2, entries 4, 5, 6). The relative reactivity of aryl halide towards the metal centre decreases in the order: I > Br ≫ Cl. Aryl halides activated by the proximity of electron-withdrawing groups are

**Table 2** Reactivity of SBA-15–EDTA–Pd(11) catalyst for Suzuki reaction[a]

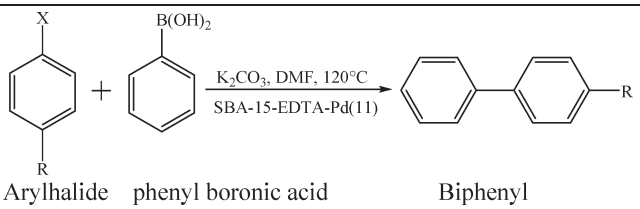


Arylhalide phenyl boronic acid Biphenyl

| S. no | Aryl halide | Product | Time (h) | Yield (%) | TON |
|---|---|---|---|---|---|
| 1 | 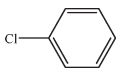 | 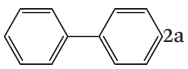 2a | 30 | 71 | 81 |
| 2 | 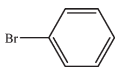 | 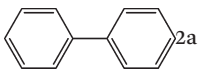 2a | 8 | 83 | 94 |
| 3 | 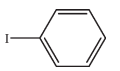 | 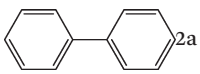 2a | 5 | 98 | 128 |
| 4 | 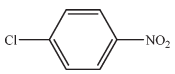 | 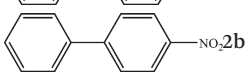 2b | 6 | 98 | 128 |
| 5 | 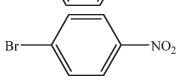 | 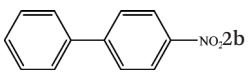 2b | 6 | 99 | 130 |
| 6 | 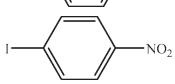 | 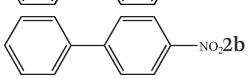 2b | 3 | 95 | 125 |
| 7 | 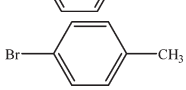 | 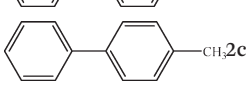 2c | 9 | 96 | 109 |
| 8 | 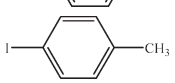 | 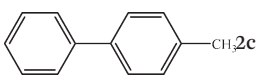 2c | 7 | 94 | 107 |
| 9 | 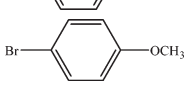 | 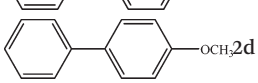 2d | 9 | 89 | 101 |
| 10 | 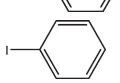 | 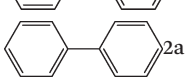 2a | 1 | 99[b] | 130 |

[a] Reaction conditions: (1.5 mmol) arylboronic acid, (1 mmol) aryl halide, (3 mmol) potassium carbonate (base), 3.5 ml DMF with (15 mg) heterogeneous SBA-15–EDTA–Pd(11) catalyst, temperature 120 °C. [b] Carried out in homogeneous catalyst EDTA–Pd. (3 mol%).

more reactive to the oxidative addition than those with donating groups, thus allowing the use of electron deficient halides, such as 4-chloronitrobenzene for the cross-coupling reaction. Further, aryl iodides are more reactive than the bromides and chlorides. The substituent effect in the aryl iodides appeared to be less significant than in the aryl chlorides and bromides.

Subsequently, the electron rich aryl halides also show moderate to excellent reactivity (89–96% yield) in the formation of the corresponding products (4-methylbiphenyl, 4-methoxybiphenyl) in the Suzuki coupling reaction under similar reaction conditions. The electron rich *para* substituted aryl halides, such as 4-bromotoluene, 4-iodotoluene 4-bromoanisole, with boronic acid afforded 96%, 94%, and 89% yields after 9 h, 7 h, 9 h, respectively (Table 2, entries 7, 8, 9). The coupling reaction of chloronapthalene with phenyl boronic acid was investigated under similar reaction conditions, but no desired coupled product was obtained, even after 24 h of reaction time. In addition, the catalytic activity of the SBA-15–EDTA–Pd(11) was compared with a homogeneous counterpart. The product yield over SBA-15–EDTA–Pd(11) and EDTA–Pd were found to be 98 and 99 wt.% conversion in 5 h and 1 h, respectively (Table 2, entries 3 and 10).

### Sonogashira reactivity

The original Sonogashira reaction often required a very dry organic solvent, inert atmosphere, strong base, prolonged reaction time and a phosphine containing catalyst. Generally a copper co-catalyst was needed in the Sonogashira coupling reaction. However, the addition of copper, although beneficial in terms of increasing the reactivity of the system added some shortcomings, the principal being the necessity of avoiding the presence of oxygen in order to block the undesirable alkyne homocoupling through a copper mediated Hay/Glaser reaction. The copper–acetylides formed *in situ* could undergo an oxidative dimerization to give diaryldiacetylenes when they are exposed to air or an oxidant (a reaction known as the Glaser coupling). These byproducts are generally difficult to separate from the desired products. Furthermore, the copper acetylide is a potential explosive reagent. To address such a problem, a solution was to eliminate the copper in the so-called "copper-free" Sonogashira reaction.[21]

Here, we have shown that the synthesized catalyst SBA-15–EDTA–Pd(11) catalyst can be effectively handled in phosphine and copper free conditions for the Sonogashira coupling reaction. Without the involvement of copper, there are even fewer mechanistic suggestions to be found in a homogeneous catalytic system.[22] The heterogeneous Sonogashira coupling of phenyl acetylene with an aryl halide may proceed through a catalytic cycle analogous to that proposed for the homogeneous palladium catalysts.

In the first step the catalytic cycle is initiated by an oxidative addition of the aryl halide (Ar–X) to species (**1**), forming the oxidative addition adduct reaction intermediate (**2**) species. The second step is the activation of the terminal alkyne. Because no copper salt was employed, and the base must be strong enough to abstract a proton from the alkyne, a transmetalation step could be excluded.[21] The terminal alkyne C–H bond activation is accomplished by the coordination of the alkyne to the SBA-15-L-($Ar^I$–Pd–X) (**3**) complex. Upon coordination, the C–H bond is weakened, and H–X is removed from the SBA-15-L-($Ar^I$–Pd–X) (**3**) in the presence of a base (triethylamine) (**6**) to form the reaction intermediate (**5**) with the subsequent byproduct of triethylamine halide (**7**). In the last step of the reaction mechanism a reductive elimination of diphenylacetylene $Ar^I$–Ar (**7**) from the unsymmetrical intermediate (**6**) regenerates the SBA-15-L-(Pd) complex.[21]

In order to probe the role of the solvent in the Sonogashira coupling reactions, a series of bases such as NaOH, $Na_2CO_3$, $K_2CO_3$, $NEt_3$ and $NaHCO_3$ were screened in the reaction.[21] Among all the organic bases used, triethylamine ($NEt_3$) was found to be most reactive in comparison to the inorganic bases. The order of reactivity of iodobenzene in the presence of various bases could be arranged in the decreasing order as: $NEt_3$ (100%) > $K_2CO_3$ (58%) > $Na_2CO_3$ (45%) > NaOH (35%) > $NaHCO_3$ (10%). It is clear from the comparison that the triethylamine base plays a highly active role in the Sonogashira coupling reaction (Fig. S8†). These organic bases were superior to inorganic bases such as $K_2CO_3$, $Na_2CO_3$, NaOH, $NaHCO_3$, and $NEt_3$. This may be due to the partial inhomogeneity of the inorganic bases with the organic substrate, reagent and solvent, which lowered the conversion and increased the reaction times compared to the organic bases (10–100% in 2 h).

After optimizing the reaction parameters, various substituted and non-substituted aryl halides were also investigated in the Sonogashira coupling reaction between iodobenzene and phenyl acetylene, in Cu free reaction conditions and the results are summarized in Table 3.

Various aryl halides were coupled with phenylacetylene in the presence of SBA-15–EDTA–Pd(11), triethylamine (3 mmol) and with DMF as a solvent at 120 °C (Table 3). As evident from the Table 3, all the substituted and non-substituted aryl halides reacted with phenyl acetylene under mild reaction conditions to give their corresponding products (Table 3, entries 1–8). Monosubstituted aryl halides, such as chlorobenzene, bromobenzene and iodobenzene, with phenyl acetylene gave the coupled product (biphenyl) in 75%, 85%, 100% yields with a TON of 85, 97, 114, respectively. As discussed earlier, the chlorides show a poor reactivity compared to the bromides and iodides under similar reaction conditions. As is clear from the Table 3, the Sonogashira coupling reactions proceeded quickly with the aryl iodides and bromides, in comparison to the chlorides (Table 3, entries 1, 2, 3).

The electron withdrawing (deficient) nitro ($-NO_2$) bearing aryl halides, such as 4-chloronitrobenzene, 4-bromonitrobenzene, 4-iodonitrobenene, with phenyl acetylene, gave the coupled product 4-nitrobiphenyl in 99%, 98%, 100% yields and 113, 112, 114 TON, respectively. From the catalytic cycle point of view in the Sonogashira coupling reaction, the oxidative addition of the aryl halide to the Pd metal centre result in the transition state (**3**) in the first step. The relative reactivity decreases in the order of I > Br ≫ Cl. Aryl halides activated by the

 

**Table 3** Reactivity of SBA-15–EDTA–Pd(11) catalyst for Sonogashira reaction[a]

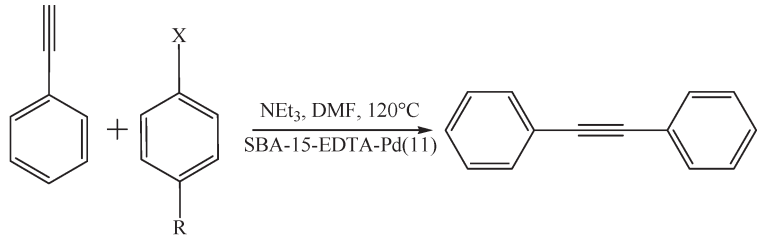


Phenylacetylene Arylhalide diphenylacetylene

| S. no | Aryl halide | Product | Time (h) | Yield (%) | TON |
|---|---|---|---|---|---|
| 1 | 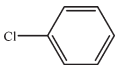 | 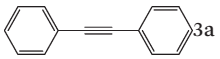 3a | 24 | 75 | 85 |
| 2 | 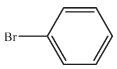 | 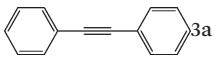 3a | 8 | 85 | 97 |
| 3 | 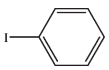 | 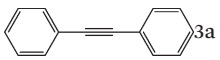 3a | 6 | 100 | 114 |
| 4 | 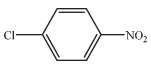 | 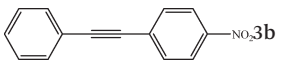 3b | 1 | 99 | 113 |
| 5 | 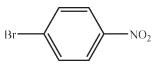 | 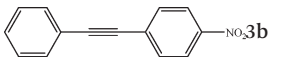 3b | 7 | 98 | 112 |
| 6 | 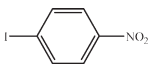 | 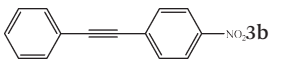 3b | 1 | 100 | 114 |
| 7 | 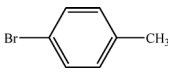 | 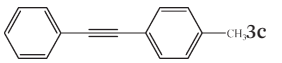 3c | 9 | 89 | 101 |
| 8 | 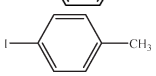 | 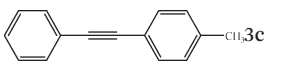 3c | 7 | 99 | 113 |

[a] Reaction conditions: (1.15 mmol) phenyl acetylene, (1 mmol) aryl halide, (3 mmol) triethylamine (base), 3.5 ml DMF with (15 mg) heterogeneous SBA-15–EDTA–Pd(11) catalyst, temperature 120 °C.

proximity of electron-withdrawing groups are more reactive to the oxidative addition than those with donating groups. Electron withdrawing groups increase the reactivity of aryl halides in the coupling reaction; which is clear from Table 3 (entries 4, 5, 6). However, the electron donating groups such as methyl bearing aryl halides like 4-bromotoluene, 4-iodotoluene with phenylacetylene, gave the corresponding products in 89% and 99% yields with 101 and 113 TON, respectively (Table 3 entries 7, 8).

Generally, electron donating bearing aryl halides show a lower reactivity in coupling reactions, since the electron density increases over the Pd intermediate (3) results in a lower feasibility of further transmetalation and the reductive elimination step, respectively. It is clear from Table 3 (entries 5–8) that aryl halides bearing methyl and nitro groups react with phenyl acetylene to give excellent yields of the corresponding biaryl, whereas the aryl chlorides possessing *para*-substituents, give good yields. Electron-rich substrates, such as 4-bromotoluene and 4-iodotoluene show lower reactivity in comparison to the electron withdrawing bearing aryl halides and take a longer reaction period for the completion of the reaction (Table 3, entries 7, 8). The coupling reaction of sterically hindered 2-chloronapthalene with phenyl acetylene did not proceed, even after a longer reaction time (24 h).

### Heterogeneity and recycling studies of catalyst SBA-15–EDTA–Pd(11)

To test if the metal was leached out from the solid catalyst during the reaction, a hot filtration test was performed. In this process the Sonogashira coupling reaction mixture was collected by filtration at the reaction temperature (120 °C) after a reaction time of 1 h, which gave a 58% conversions of iodobenzene. The residual activity of the supernatant solution was studied. It was noticed that after filtration of the SBA-15–EDTA–Pd(11) catalyst from the reaction mixture at the elevated reaction temperature (120 °C), (in order to avoid a possible recoordination or precipitation. of soluble palladium upon cooling) the coupling reactions did not proceed further. Thus, the results of the hot filtration test suggest that Pd was not being leached out from the solid catalyst during the coupling reactions. These results confirm that the palladium catalyst remains on the support even at elevated temperatures during the reaction.

Further, to evaluate the reusability, after carrying out the reaction, the mixture was filtered using a sintered glass funnel, and the residue washed with DMF (3–5 ml), dichloromethane (2–5 ml) and acetone (2–5 ml). After being dried in an oven (overnight), the catalyst could be reused directly without further purification (Fig. 9). The amount of Pd leaching into

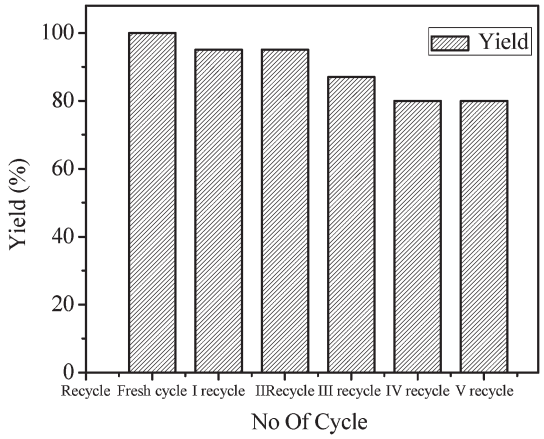


**Fig. 9** Recycling study of SBA-15–EDTA–Pd(11) catalyst.

solution for the Suzuki reactions were detected through ICP. The amount of lost Pd for the reaction was less than 1.0 weight % of the total Pd content. Even though a small amount of Pd loss could be detected, the catalyst still showed a relatively high reusability and stabilities for Sonogashira coupling reactions. The present study indicates that the catalyst can be recycled a number of times without losing its activity to a greater extent.

## Conclusion

In summary, a highly stable and recyclable SBA-15–EDTA–Pd catalyst has been synthesized by anchoring a Pd–EDTA complex over the inner surface of organo-functionalized SBA-15 with different wt.% loading (7%, 11%, and 15%). XRD and $N_2$ sorption analyses, which reveal the morphological and textural properties of the synthesized catalyst, confirm that the metal complex Pd–EDTA is firmly attached to the organo-modified SBA-15 support and the ordered mesoporous channel structure was retained even after multistep synthetic procedures. The TGA-DTA results reveal the thermal stability of the synthesized catalyst SBA-15–EDTA–Pd(11) at elevated temperatures. The organic moieties anchored over the surface of the SBA-15 and inside the pore wall were evident by solid state $^{13}C$ NMR spectra and FT-IR spectroscopy. Further, solid state $^{29}Si$ NMR spectroscopy provides information about the degree of silylation and functionalization with the organic moieties. The electronic environment and oxidation state of the Pd metal in the SBA-15–EDTA–Pd(11) were confirmed by XPS and DRS UV-visible techniques. Subsequently, the morphology information of the synthesized catalyst was monitored by SEM and TEM spectroscopy. The synthesized heterogeneous catalyst SBA-15–EDTA–Pd(11) was screened in the Suzuki and Sonogashira coupling reactions and shows a higher catalytic activity with a higher TON in phosphine free conditions. The present SBA-15–EDTA–Pd(11) catalytic system tolerates a broad range of functional groups of the aryl halide in both the Suzuki and Sonogashira coupling reactions, without using a phosphine ligand or Cu co-catalyst. The heterogenized solid catalyst SBA-15–EDTA–Pd(11) can be recycled efficiently and reused five times, without a major loss in activity, due to the well modified surface properties of the SBA-15 as a support.

## Experimental

SBA-15 was synthesized according to the reported procedure using tri-block P123 as a template under acidic conditions.[23] Pluronic 123 (2 g) was dissolved in a solution of HCl (60 mL of 2.0 M) and $H_2O$ (60 mL). The solution was stirred at 38 °C for 1 h. After that time, tetraethylorthosilicate (TEOS) was added, and the resultant solution was left stirring at 38 °C for a further 4 h and then aged at 100 °C for 24 h. For the surface medication, see the ESI.†

### SBA-15–Pd–EDTA synthesis

$PdCl_2$ (0.5 mmol) in 5 ml distilled water was treated with 0.186 g (0.5 mmol) of EDTA and 1 mmol of sodium carbonate ($Na_2CO_3$) and stirred to give yellow red solution. To the resultant solution, the calculated amount (1.0 g) of organo-modified SBA-15 was added, along with the slow addition of 25 ml of Millipore water.[8] The final mixture was stirred at 75 °C for 24 h and washed with distilled water and soxhlet extracted to remove the unanchored materials from the SBA-15 surface (Scheme 1D). The resultant material was named SBA-15–EDTA–Pd(11). Similarly, 7 and 15 wt.% of Pd loading were also synthesized by using corresponding amount of modified SBA-15 and $PdCl_2$ and the obtained materials were designated as SBA-15–EDTA–Pd(7), SBA-15–EDTA–Pd(11), SBA-15–EDTA–Pd(15).

### General procedure for Suzuki coupling reactions

The Suzuki reaction was carried out in a 25 ml oven dried, two necked round bottom flask, heated over a reactor with high stirring 700+ rpm. In a typical run, 1 mmol of aryl halide, 1.15 mmol of aryl boronic acid, 3 mmol potassium carbonate ($K_2CO_3$) and 15 mg of SBA-15–EDTA–Pd(11) (heterogeneous catalyst) were allowed to stir at 120 °C with the solvent DMF (3.5 ml). The reaction mixture was sampled at measured time intervals and analyzed by gas chromatography. The samples were centrifuged with high rpm before injection into a gas chromatograph.

### General procedure for Sonogashira coupling reactions

The catalyst screening for the Sonogashira coupling reaction was carried out in 25 ml oven dried, two necked round bottom flask, heated over a reactor with high stirring 700+ rpm. In a typical, run 1 mmol of aryl halide, 1.5 mmol of phenylacetylene, 3 mmol triethylamine (base) and 15 mg of SBA-15–EDTA–Pd (11) (heterogeneous catalyst) were allowed to run at 120 °C with DMF as the solvent. The reaction mixture was sampled at measured time intervals and analyzed by gas chromatography. The samples were centrifuged with high rpm before injecting into the gas chromatograph. The products were analyzed by GCMS and $^1H$, $^{13}C$ CP MAS NMR.

 

## Acknowledgements

The authors gratefully acknowledge the CSIR networking project (CSC-0125) for financial support. P.S. thanks the UGC-New Delhi, India for a Senior Research Fellowship. The authors are thankful to Dr. Satynarayana Chlikuri for the adsorption measurements (surface area) and Dr. Vinod for the XPS studies.

## Notes and references

1 (*a*) A. Dahan and M. Portnoy, *Org. Lett.*, 2003, **5**, 1197–1200; (*b*) F. X. Felpin, T. Ayad and S. Mitra, *Eur. J. Org. Chem.*, 2006, **12**, 2679–2690; (*c*) A. Cwik, Z. Hell and F. Figueras, *Adv. Synth. Catal.*, 2006, **348**, 523–530; (*d*) B. M. Choudary, S. Madhi, N. S. Chowdari, M. L. Kantam and B. Sreedhar, *J. Am. Chem. Soc.*, 2002, **124**, 14127–14136.

2 (*a*) J. Y. Ying, C. P. Mehnert and M. S. Wong, *Angew. Chem., Int. Ed.*, 1999, **38**, 56–77; (*b*) D. Zhao, J. Feng, Q. Huo, N. Melosh, G. H. Fredrickson, B. F. Chmelka and G. D. Stucky, *Science*, 1998, **279**, 548–552; (*c*) R. I. Kureshy, A. H. Khan, K. Pathak and V. Jasra, *Tetrahedron: Asymmetry*, 2005, **16**, 3562–3569.

3 (*a*) C. Amatore, A. Jutand, M. Amine and M. Barki, *Organometallics*, 1992, **11**, 3009–3013; (*b*) H. A. Dieck and R. F. Heck, *J. Org. Chem.*, 1975, **40**, 1083–1090; (*c*) C. A. Fleckenstein and H. Plenio, *Chem. Soc. Rev.*, 2010, **39**, 694–711.

4 (*a*) A. Zapf and M. Beller, *Top. Catal.*, 2002, **19**, 101–109; (*b*) L. X. Yin and J. Liebscher, *Chem. Rev.*, 2007, **107**, 133–173.

5 (*a*) V. P. W. Bohm, C. W. K. Gstottmayr, T. Weskamp and W. Herrmann, *J. Organomet. Chem.*, 2000, **595**, 186–190; (*b*) B. Tao and D. W. Boykin, *Tetrahedron Lett.*, 2002, **43**, 4955–4957; (*c*) D. A. Alonso, C. Najera and M. C. Pacheco, *Org. Lett.*, 2000, **2**, 1823–1826; (*d*) B. Bedford and C. S. Cazin, *Chem. Commun.*, 2001, 1540–1541; (*e*) G. A. Grasa, A. C. Hillier and S. P. Nolan, *Org. Lett.*, 2001, **3**, 1077–1080; (*f*) S. R. Borhade and S. B. Waghmode, *Tetrahedron Lett.*, 2008, **49**, 3423–3429.

6 (*a*) I. P. Beletskaya, V. Andrei and A. V. Cheprakov, *Chem. Rev.*, 2000, **100**, 3009–3066; (*b*) V. Polshettiwar and A. Molnar, *Tetrahedron*, 2007, **63**, 6949–6976; (*c*) S. P. Stanforth, *Tetrahedron*, 1998, **54**, 263–303.

7 (*a*) C. M. Crawforth, I. J. S. Fairlamb, A. R. Kapdi, J. L. Serrano, R. J. K. Taylor and G. Sanchez, *Adv. Synth. Catal.*, 2006, **348**, 405–412; (*b*) M. Lamblin, L. N. Hardy, J. C. Hierso, E. Fouquet and F. X. Felpin, *Adv. Synth. Catal.*, 2010, **352**, 33–79; (*c*) X. F. Wu, H. Neumann and M. Beller, *Chem. Commun.*, 2011, **47**, 7959–7961.

8 N. Dmitri, D. N. Korolev and N. A. Bumagin, *Tetrahedron Lett.*, 2005, **46**, 5751–5754.

9 (*a*) C. Yu, B. Tian, J. Fan, G. D. Stucky and D. Zhao, *J. Am. Chem. Soc.*, 2002, **124**, 4556–4557; (*b*) J. D. Galo, A. A. S. Illia, C. Sanchez, B. Lebeau and J. Patarin, *Chem. Rev.*, 2002, **102**, 4093–4138.

10 (*a*) M. D. Alba, Z. Luan and J. Klinowski, *J. Phys. Chem.*, 1996, **100**, 2178–2182; (*b*) A. B. Bourlinos, T. Karakoatas and D. Petridis, *J. Phys. Chem. B*, 2003, **107**, 920–925.

11 Y. Jiang, Q. Gao, H. Yu, Y. Chen and F. Deng, *Microporous Mesoporous Mater.*, 2007, **103**, 316–324.

12 M. Kaplun, A. Nordin and P. Persson, *Langmuir*, 2008, **24**, 483–489.

13 H. Yoshitake, T. Yokoi and T. Tatsumi, *Chem. Mater.*, 2002, **14**, 4603–4610.

14 P. Chidambaram and A. P. Singh, *Appl. Catal., A*, 2006, **310**, 79–90.

15 D. S. Shephard, W. Zhou, T. Maschmeyer, J. M. Matters, C. L. Roper, S. Parsons, B. F. G. Johnson and M. J. Duer, *Angew. Chem., Int. Ed.*, 1998, **37**, 2719–2723.

16 A. Gniewek, A. M. Trzeciak, J. J. Ziółkowski, L. K. Epinski, J. Wrzyszcz and W. Tylus, *J. Catal.*, 2005, **229**, 332–343.

17 Z. Gao, Y. Feng, F. Cui, Z. Hua, J. Zhou, Y. Zhu and J. Shi, *J. Mol. Catal. A: Chem.*, 2011, **336**, 51–57.

18 D. S. Martin, R. M. Rush and G. A. Robin, *Inorg. Chem.*, 1980, **19**, 1705–1709.

19 (*a*) M. M. Manas, M. Perez and R. Pleixats, *J. Org. Chem.*, 1996, **61**, 2346–2351; (*b*) N. Miyaura, K. Yamada, H. Suginome and A. Suzuki, *J. Am. Chem. Soc.*, 1985, **107**, 972–980.

20 B. Zhang, J. Song, H. Liu, J. Shi, J. Ma, H. Fan, W. Wang, P. Zhang and B. Han, *Green Chem.*, 2014, **16**, 1198–1201.

21 (*a*) T. Ljungdahl, T. Bennur, A. Dallas, H. Emtenas and J. Mårtensson, *Organometallics*, 2008, **27**, 2490–2498; (*b*) T. Ljungdahl, K. Pettersson, B. Albinsson and J. Mårtensson, *J. Org. Chem.*, 2006, **71**, 1677–1687.

22 (*a*) J. Cheng, Y. Sun, F. Wang, M. Guo, J. H. Xu, Y. Pan and Z. Zhang, *J. Org. Chem.*, 2004, **69**, 5428–5432; (*b*) B. H. Lipshutz, D. W. Chung and B. Rich, *Org. Lett.*, 2008, **10**, 3793–3796.

23 D. Zhao, J. Feng, Q. Huo, N. Melosh, G. Fredrickson, B. Chmelka and G. Stucky, *Science*, 1998, **279**, 548–552.